

Monolithic self-sustaining nanographene sheet grown using plasma-enhanced chemical vapor deposition

Wakana Takeuchi^{*1}, Keigo Takeda¹, Mineo Hiramatsu², Yutaka Tokuda³, Hiroyuki Kano⁴, Shigeru Kimura⁵, Osami Sakata⁵, Hiroo Tajiri⁵, and Masaru Hori¹

¹Department of Electrical Engineering and Computer Science, Nagoya University, Chikusa, Nagoya 468-8603, Japan

²Department of Electrical and Electronic Engineering, Meijo University, Tempaku, Nagoya 468-8502, Japan

³Department of Electrical and Electronics Engineering, Aichi Institute of Technology, Yakusa, Toyota 470-0392, Japan

⁴NU Eco-Engineering Co., Ltd., Kurozasa, Miyoshi, Nishikamo 470-0201, Japan

⁵Japan Synchrotron Radiation Research Institute (JASRI)/SPRING-8, Kouto, Sayo 679-5198, Japan

Received 7 May 2009, revised 20 August 2009, accepted 20 August 2009

Published online 18 September 2010

PACS 52.77.Dq, 61.46.-w, 78.30.Na, 81.15.Gh

Corresponding author: e-mail w_takeuchi@nagoya-u.jp

We have fabricated carbon nanowalls (CNWs) composed of monolithic self-sustaining nanographene sheets standing vertically on a Si substrate, using plasma-enhanced chemical vapor deposition with a C₂F₆/H₂ mixture. The crystallinity, evaluated by Raman spectroscopy and synchrotron X-ray surface

diffraction, and the electrical properties of the CNWs were improved by introducing O₂ gas into the source gas mixture during the CNW growth process. The temperature dependence of the resistivity of the CNW films exhibited semiconductor behavior.

© 2010 WILEY-VCH Verlag GmbH & Co. KGaA, Weinheim

1 Introduction Two-dimensional (2D) graphene sheets, which range from a single layer to stacks of a few layers, have attracted great interest for use in next-generation electronic devices. Few-layer graphene sheets have been reported to have high mobilities of 10 000–15 000 cm² Vs⁻¹ and a band gap of 0.26 eV [1, 2]. However, the primary method for isolating graphene, i.e., micromechanical cleavage of graphite, cannot be easily scaled up for large-scale applications.

Recently, several reports have been published on the growth of carbon nanowalls (CNWs), which are 2D carbon nanostructures comprising of planar graphene layers standing almost vertically on a substrate [3–6]. CNWs can be described as 2D graphite nanostructures with edges and they have a wall-like structure with an ultrahigh aspect ratio. Since CNWs essentially consist of graphene sheets, they are expected to have high mobilities and large sustainable current densities. Therefore, CNWs are considered to be one of the most promising carbon materials for nanoscale electronic devices.

CNWs have been synthesized by various chemical vapor deposition (CVD) techniques, including microwave plasma-enhanced chemical vapor deposition (PECVD) [3], radio-

frequency inductively coupled PECVD [4], and hot-filament CVD [5]. We have fabricated CNWs by fluorocarbon PECVD with hydrogen (H) radical injection. This method has the potential to control the morphology of CNWs, such as the thickness and the spacing between the walls [6, 7]. Recently, we fabricated nitrogen-doped CNWs by injecting N₂ gas into the processing plasma and evaluated their electrical conduction properties [8].

CNWs have been reported to consist of nanodomains that are a few tens of nanometers in size [9] and individual CNWs were found to have many edges and defects [10]. Therefore, in order to fully exploit the potential of graphene and to develop next-generation electronic devices, reliable methods are required for fabricating graphene sheets with high crystallinity. In our previous study, O₂ plasma was used to remove the carbon-related coating on the chamber wall for the fabrication of CNWs with high reproducibility [11]. In contrast, the addition of small amount of CO₂ or H₂O to the hydrocarbon plasma is effective to etch disordered carbon species [12, 13]. Carbon–oxygen reactions on various kinds of carbon surfaces have been studied [14]. In some cases, the trigonal bond of carbon at the edges of basal planes of the crystallites and defects within the basal plane act as

nucleation sites for undesirable nanostructured carbon. These nucleation sites can be eliminated by reacting with atomic oxygen to form volatile by-products such as CO and CO₂. Thus, using carbon–oxygen reactions would enable us to synthesize carbon materials that have larger crystallite sizes, higher crystallite alignment, and higher purity.

In this study, CNW films were fabricated using PECVD with a C₂F₆/H₂ mixture. We investigated the effect of O₂ gas addition to the process gas mixture of C₂F₆/H₂ on the structure and electrical properties of CNW films. We found that the crystallinity of vertically standing graphene sheets is improved by introducing O₂ into the plasma used for CNW growth, and that the well-defined CNW films synthesized by PECVD exhibit semiconductor behavior.

2 Experimental CNW films were fabricated using PECVD with H radical injection with a mixture of C₂F₆ and H₂. The radical-injection PECVD system consists of a parallel-plate VHF (100 MHz) capacitively coupled plasma (CCP) with C₂F₆ and a surface-wave-excited microwave H₂ plasma as a remote H radical source. Details of the radical-injection PECVD system are provided elsewhere [8, 11]. The C₂F₆ and H₂ flow rates were maintained at 50 and 100 sccm, respectively. O₂ was introduced into the CCP region at flow rates of 0–5 sccm and the total pressure was maintained at 160 Pa.

3 Results and discussion Figure 1a and b shows cross-sectional scanning electron microscopy (SEM) images of the CNW films, and the insets show top-view SEM images of the same CNW films. Figure 1a shows SEM images of a typical CNW film grown for 30 min on a Si substrate using a

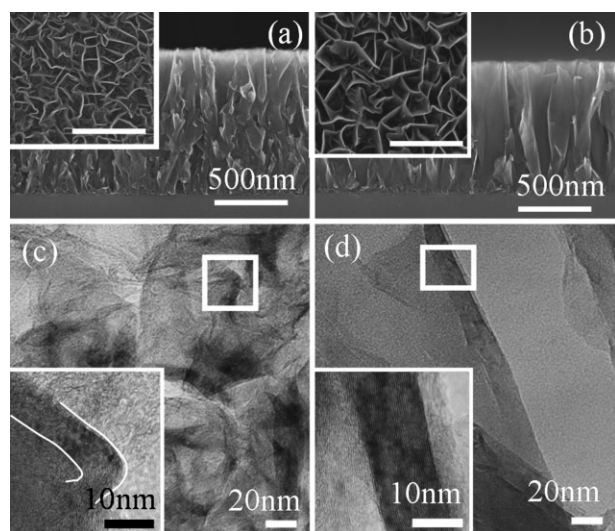


Figure 1 Cross-sectional SEM images of (a) CNW film grown on a Si substrate using C₂F₆/H₂ and (b) CNW film grown using C₂F₆/H₂ with additional O₂ gas, together with SEM top-view images of identical CNW films as insets. TEM images of (c) CNWs grown without any additional gas and (d) CNWs grown with additional O₂, together with magnified images of square areas as insets, showing layered graphene structures of CNWs.

C₂F₆/H₂ mixture without O₂. These images show slightly branching 2D carbon sheets standing almost vertically on the substrate. The CNW height, which is equivalent to the CNW film thickness, was approximately 1 μm. Figure 1b shows SEM images of CNWs grown for 40 min with the addition of O₂ at a flow rate of 5 sccm. These CNWs exhibit less branching than those produced without O₂ so that monolithic graphene sheets were obtained; however, the growth rate was reduced by approximately 33%. CNW films grown with O₂ had larger plane sheets with wider interspaces than those grown without O₂.

Cross-sectional transmission electron microscope (TEM) images of CNW films grown without and with O₂ are shown in Fig. 1c and d, respectively. Small overlapping multi-layered graphene domains with random orientations were observed for CNWs grown without O₂ (Fig. 1c). By contrast, monolithic self-sustaining graphene sheets larger than 200 nm in size were clearly observed in the CNWs grown with O₂ (Fig. 1d). The insets show magnified images of the areas enclosed by squares in Fig. 1c and d; these images allow the fine structure of the CNWs to be assessed. The inset of Fig. 1c clearly shows a bent multi-layered graphene structure with a thickness of approximately 9 nm in the case of CNW grown without O₂. On the other hand, a highly orientated, smooth multi-layered graphene structure was clearly obtained in the CNW grown with O₂ (inset of Fig. 1d).

CNW grown without and with O₂ gas addition were also characterized by Raman spectroscopy to investigate the influence of O₂ gas addition on the structural property of CNWs. Raman spectroscopy is a powerful tool and widely applied to determine the structural properties of various forms of carbon nanostructures. Raman spectra for the deposits were measured at room temperature with a triple monochromator (Jobin Yvon, Ramanor T64000) using the 514.5 nm line of an Ar laser in the spectral range from 1200 to 1800 cm⁻¹. Figure 2a shows the Raman spectra of the CNW films grown with different O₂ flow rates. The Raman spectra of all the CNW films have a G-band peak at 1584 cm⁻¹ indicating the formation of a graphitized structure, and a D-band peak around at 1350 cm⁻¹ corresponding to the disorder-induced phonon mode. Usually, the G-band peak is accompanied by a shoulder peak at 1620 cm⁻¹ (D'-band). The D'-band is associated with finite-size graphite crystals [10]. The strong D-band and D'-band peaks suggest a more nanocrystalline structure and the presence of graphene edges and defects, which are features of CNWs. Figure 2b shows the ratio of the peak intensity of the D-band to that of the G-band (I_D/I_G). The I_D/I_G decreased with an increase in the O₂ flow rate, indicating that the O₂ addition improved the crystallinity of CNWs by suppressing the second nucleation, resulting in the improvement of the crystallinity of CNW films.

The crystallinity of CNWs was analyzed using synchrotron X-ray surface diffraction at grazing incidence and exit at the beamline BL13XU of SPring-8 [15]. The X-ray beam was incident on the CNW film samples at glancing angles of 0.05° and 0.3° relative to the substrate surface; these incident angles were, respectively, used to evaluate the crystallinity of the

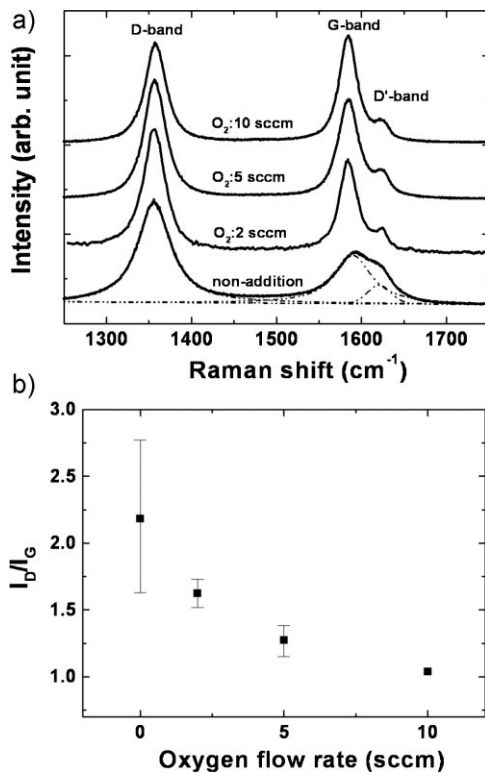


Figure 2 (a) Raman spectra of CNW film without and with O_2 addition. (b) The peak intensity ratio of D-band to G-band as a function of O_2 gas addition.

vertically standing CNWs near the surface region, and to evaluate the CNWs, including the interface between the CNWs and the Si substrate. Figure 3 shows the diffraction patterns of CNW film samples recorded at the glancing angle of 0.3° . An intense 002 Bragg peak, the plane of which is normal to the substrate, is at $2\theta = 16.9^\circ$ and there are also weak 100/101, 004, and 110 Bragg peaks. The interlayer spacing

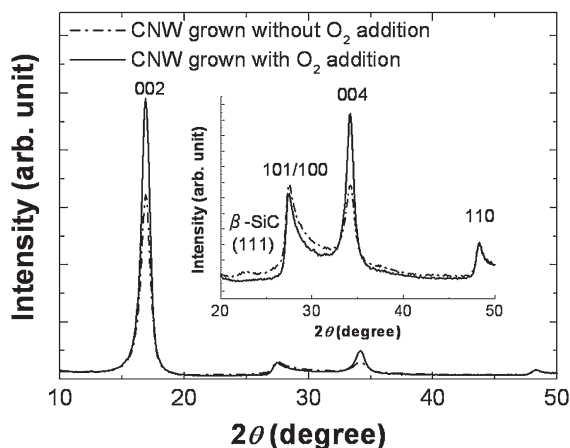


Figure 3 SR X-ray diffraction patterns of CNW films grown with and without O_2 addition; various conditions measured at beam line BL13XU of SPring-8. The inset is a magnified profile in the 2θ region of $20\text{--}50^\circ$.

d_{002} was determined from the 002 peak by applying Bragg's law with a wavelength of $\lambda = 0.1003$ nm. It was found to be 0.342 nm for all samples, which is slightly larger than that of bulk graphite (0.335 nm), but is the same as that of the layered carbon fluorides, the F atoms of which are reduced by the abstract reaction with hydrogen [16]. The interlayer spacing in the present study may be large due the presence of F atoms, although their concentration in the CNWs grown with O_2 was very low. The average thickness of the CNWs was determined from the mean crystallite size (L_c), which is calculated from the 002 peak width using the Scherrer equation [17]. The values of L_c for CNWs grown without and with O_2 were estimated to be 9.4 and 13.0 nm, respectively; these values are almost the same as the wall thicknesses evaluated by TEM.

We evaluated the degree of vertical structure of the CNWs using the ratio of the 002 peak intensity ratio to the 100/101 integrated intensity ratio ($I_{002}/I_{100/101}$). The values of $I_{002}/I_{100/101}$ for CNWs grown without and with O_2 were found to be 4.8 and 10.4, respectively. The $I_{002}/I_{100/101}$ ratio of CNWs grown with O_2 was twice that of CNWs grown without O_2 , indicating that orientation of the vertically standing graphene sheets was improved by introducing O_2 into the plasma for CNW growth with PECVD with a C_2F_6/H_2 mixture. A weak broad peak at $2\theta = 22.8^\circ$ was observed only for CNWs grown without O_2 when the glancing angle was 0.3° . This peak was not observed at the glancing angle of 0.05° , suggesting it is related to the interface phase near the substrate. This peak is attributed to β -SiC (111), which has an amorphous structure and is formed between the CNWs and the Si substrate. This interface peak was not observed for the CNWs grown with O_2 .

A quartz substrate was used to evaluate the electrical properties of the CNW films. After synthesizing the CNW films on a quartz substrate, four aluminum (Al) contacts were symmetrically positioned on the CNW film for Hall measurements by the van der Pauw method [18]. The Hall coefficients of the CNW film samples grown with and without O_2 were measured using a resistivity/Hall measurement system. In this measurement, it was assumed that the CNW film is a plane membrane from a macroscopic standpoint and that the current flows uniformly on the surface between the contacts. Before performing the Hall measurement, we confirmed that the Al electrodes are ohmic

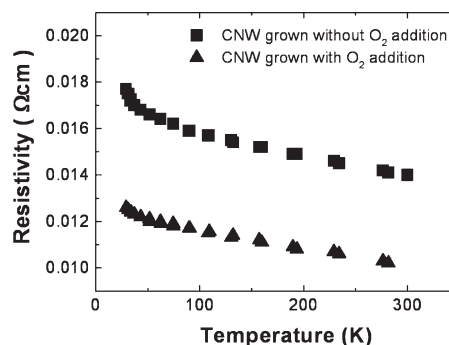


Figure 4 Variation in resistivities of CNW films as a function of temperature.

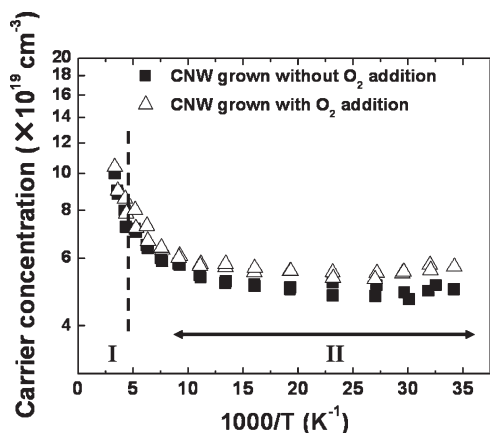


Figure 5 Carrier concentration of CNW films as a function of the reciprocal of the temperature. I and II correspond to the intrinsic region and the saturation region, respectively.

contacts for the CNW film. Figure 4 shows the resistivity variation of the CNW films as a function of temperature, which was derived from the Hall measurement. The resistivity of CNW film was reduced by approximately 30% as a result of O₂ addition during the CNW growth process. The resistivity of all the CNW films decreased with an increase in the measured temperature, indicating the semiconductor behavior of the CNW films.

Figure 5 shows the carrier concentration of CNW films as a function of the reciprocal of the temperature. The carrier concentration of the CNW films showed the flat profile at low temperatures up to 100 K (1000/T = 10). As the temperature was increased up to room temperature (1000/T: lower than 10), the carrier concentration drastically increased. The regions I and II in Fig. 5 indicate the intrinsic and the saturation regions, respectively. The carrier concentration behavior of CNW film grown without O₂ addition showed almost the same tendency as that of the CNW grown with O₂ addition. Thus, the carrier generation mechanism for CNW films grown with and without O₂ is considered to be the same. However, the carrier concentration of CNW film grown with O₂ was slightly higher than that of CNW film grown without additional gas. The band gap can be obtained from the slope of the intrinsic range I in Fig. 5. Thus, the band gap of CNW film was estimated from the region I at 300 K, which was approximately 80 meV for both CNW films grown without and with O₂ addition. However, the intrinsic region was not clearly observed in Fig. 5, because the temperature range for the present Hall measurement system was limited up to room temperature. The slope in region I for the measured curve in Fig. 5 is still on the rise at 300 K. Therefore, the band gap of CNW film was expected larger than 80 meV.

The resistivity and carrier concentration derived in this study reflect the electrical property of the bulk CNW film comprising the web of nanographene sheets with interspaces. These values could be useful for the design and evaluation of electronic devices using bulk CNW films. On the other hand,

the carrier concentration and mobility as well as the band gap inside the individual monolithic CNW sheets are of great interest for realizing nanographene devices. We are currently evaluating the electrical properties of individual CNW sheets.

CNW films grown with additional O₂ were characterized by secondary ion mass spectrometry (SIMS) to investigate the effect of O₂ addition to the C₂F₆/H₂ plasma on the atomic composition of CNWs. The depth distributions of the relative atomic composition ratios [O]/[C] and [F]/[C] were measured using a 10 keV Cs⁺ primary beam for sputtering. The relative atomic composition ratios [O]/[C] in the CNWs grown with and without O₂ were found to be almost the same at 1.6 × 10⁻⁴ based on the SIMS depth profile (data not shown), suggesting that O atoms were not incorporated in the CNWs grown with O₂. On the other hand, the relative atomic composition ratio [F]/[C] in the CNWs grown with O₂ was 1.7 × 10⁻⁵, while it was 7.1 × 10⁻⁴ in the CNWs grown without O₂, indicating that O atoms scavenge F atoms by forming volatile COF₂ molecules during the growth of CNWs [19]. The electrical conduction of graphite with a fluorine junction (CF)_n was found to be disturbed since the excess charge induced by the F atoms reduces the graphite π density [20]. The bent multi-layered graphene structure shown in Fig. 1a and c include many defects as well as impurities such as residual F atoms. These residual F atoms act as impurities and F-induced defects in CNWs will affect electrical conduction. As a result of O₂ addition to the C₂F₆/H₂ plasma, the F atoms in CNWs were effectively eliminated, while the O atoms were not incorporated in the CNW film. This suggests that oxygen etch F atoms and small graphitic fragments, thereby contributing to the higher graphitization and improving the crystallinity and electrical conduction to form highly oriented monolithic graphene sheets.

4 Conclusions We synthesized CNW films composed of monolithic self-sustaining nanographene sheets vertically standing on the substrate. Synchrotron X-ray surface diffraction measurements revealed that the crystallinity of vertical graphene sheets was improved by introducing O₂ into the plasma used for CNW growth. The resistivity of the CNW film decreased with an increase in the temperature, indicating that the CNW films exhibit semiconductor behavior. The current results demonstrate that CNWs consisting of vertical, monolithic self-sustaining nanographene sheets have great potential for application in next-generation electronic devices.

Acknowledgements The synchrotron radiation experiments were conducted on the BL13XU of SPring-8 under the Priority Nanotechnology Support Program administrated by JASRI (Proposal No. 2007B1752). Part of this work was supported by a Grant-in-Aid for Scientific Research in a Priority Area (Nos. 18063019 and 18063011) from the Japanese Ministry of Education, Culture, Sports, Science, and Technology. The authors would like to thank K. Nakatsu and J. Yamagata for the measurements and a fruitful discussion. This study was partly supported by Sumika Chemical Analysis Service, Ltd.

References

- [1] K. S. Novoselov, A. K. Geim, S. V. Morozov, D. Jiang, Y. Zhang, S. V. Dubonos, I. V. Grigorieva, and A. A. Firsov, *Science* **306**, 666 (2004).
- [2] S. Y. Zhou, G.-H. Gweon, A. V. Fedorov, P. N. First, W. A. de Heer, D.-H. Lee, F. Guinea, A. H. Castro Neto, and A. Lanzara, *Nature Mater.* **6**, 770 (2007).
- [3] Y. H. Wu, P. W. Oiao, T. C. Chong, and Z. X. Shen, *Adv. Mater.* **14**, 64 (2002).
- [4] J. J. Wang, M. Y. Zhu, R. A. Outlaw, X. Zhao, D. M. Manos, B. C. Holloway, and V. P. Mammanna, *Appl. Phys. Lett.* **85**, 1265 (2004).
- [5] N. G. Shang, F. C. K. Au, X. M. Meng, C. S. Lee, I. Bello, and S. T. Lee, *Chem. Phys. Lett.* **358**, 187 (2002).
- [6] M. Hiramatsu, K. Shiji, H. Amano, and M. Hori, *Appl. Phys. Lett.* **84**, 4708 (2004).
- [7] M. Hiramatsu and M. Hori, *Jpn. J. Appl. Phys.* **45**, 5522 (2006).
- [8] W. Takeuchi, M. Ura, M. Hiramatsu, Y. Tokuda, H. Kano, and M. Hori, *Appl. Phys. Lett.* **92**, 213103 (2008).
- [9] K. Kobayashi, M. Tanimura, H. Nakai, A. Yoshimura, H. Yoshimura, K. Kojima, and M. Tachibana, *J. Appl. Phys.* **101**, 094306 (2007).
- [10] S. Kurita, A. Yoshimura, H. Kawamoto, T. Uchida, K. Kojima, M. Tachibana, P. Molina-Morales, and H. Nakai, *J. Appl. Phys.* **97**, 104320 (2005).
- [11] S. Kondo, M. Hori, K. Yamakawa, S. Den, H. Kano, and M. Hiramatsu, *J. Vac. Sci. Technol. B* **26**, 1294 (2008).
- [12] H. Chatei, M. Belmahi, M. B. Assouar, L. Le Brizoual, P. Bourson, and J. Bougdira, *Diamond Relat. Mater.* **15**, 1041 (2006).
- [13] M. Hiramatsu, M. Inayoshi, K. Yamada, E. Mizuno, M. Nawata, M. Ikeda, M. Hori, and T. Goto, *Rev. Sci. Instrum.* **67**, 2360 (1996).
- [14] P. L. Walker, Jr., R. L. Taylor, and J. M. Ranish, *Carbon* **29**, 411 (1991).
- [15] S. Goto, N. Ikeda, K. Inoue, H. Kimura, and M. Yabashi, *SPring-8 Beamline Handbook, Ver. 3* (Japan Synchrotron Radiation Research Institute, Hyogo, Japan, 2004), p. 48.
- [16] Y. Sato, H. Watano, R. Hagiwara, and Y. Ito, *Carbon* **44**, 664 (2006).
- [17] A. Sharama, T. Kyotani, and A. Tomita, *Carbon* **38**, 1977 (2000).
- [18] L. J. van der Pauw, *Philips Tech. Rev.* **20**, 220 (1958).
- [19] H.-P. Hsueh, R. T. McGrath, B. J. Felker, B. S. Langan, J. G. Langan, and E. J. Karwacki, *J. Vac. Sci. Technol. B* **19**, 1346 (2001).
- [20] J.-C. Charlier, X. Gonze, and J.-P. Michenaud, *Phys. Rev. B* **47**, 16162 (1993).